Journal of Electron Spectroscopy and Related Phenomena 246 (2021) 147013

Contents lists available at ScienceDirect

Journal of Electron Spectroscopy and Related Phenomena

journal homepage: www.elsevier.com/locate/elspec

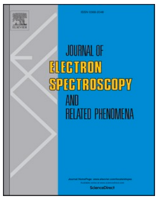

The magnetic order in multiferroic $DyMnO_3$

Jenn-Min Lee [a,b], Shih-Wen Huang [a,c,d,*], Horng-Tay Jeng [e], Yu-Cheng Shao [f,c], L. Andrew Wray [g], Jin Ming Chen [b], Ruimin Qiao [c], Wanli Yang [c], Jiunn-Yuan Lin [h], Robert W. Schoenlein [d], Yi-De Chuang [c,*]

[a] MAX IV Laboratory, Lund University, P.O. Box 118, 221 00 Lund, Sweden
[b] National Synchrotron Radiation Research Center, Hsinchu 30076, Taiwan
[c] Advanced Light Source, Lawrence Berkeley National Laboratory, Berkeley, CA 94720, USA
[d] Materials Sciences Division, Lawrence Berkeley National Laboratory, Berkeley, CA 94720, USA
[e] Department of Physics, National Tsing Hua University, Hsinchu 30013, Taiwan
[f] Department of Physics, Tamkang University, Taipei 25137, Taiwan
[g] Department of Physics, New York University, New York, NY 10003, USA
[h] Institute of Physics, National Chiao Tung University, Hsinchu 300, Taiwan

ARTICLE INFO

Keywords:
Multiferroic
Resonant X-ray scattering

ABSTRACT

With flexibility in tuning their electric and magnetic properties, multiferroics can be used in information exchange and storage in ways that are very different from the present electronic materials. Here we use resonant soft X-ray scattering spectroscopy to study the *F*-type $(0, \tau, 0)$ and *C*-type (0, $1–2\tau$, 0) diffraction peaks from sinusoidal antiferromagnetic spin order in multiferroic $DyMnO_3$. By comparing the temperature dependence of ordering wave vectors τ, peak intensities *I*, and correlation lengths λ measured at Mn L_2-, O *K*-, and Dy M_5-edges, we show that the nearly perfect locking between the ordering wave vectors from Dy 4*f* states and Mn 3*d* orbitals manifesting the second harmonic diffraction peak implies the notable orbital involvement in the coupling between Mn and Dy spins. Our DFT calculations further suggest that the lattice response to different antiferromagnetic ground states (A-type versus E-type) is much weaker in $TbMnO_3$, in agreement with previous claim that the symmetric exchange interaction can be an important factor for understanding the ferroelectricity in $DyMnO_3$ than in $TbMnO_3$.

1. Introduction

In response to the growing demands on energy to sustain the human civilization, modern electronic devices are becoming more powerful, compact, and energy efficient. However, this evolutionary trend for electronic devices will soon reach the bottleneck around nm critical dimension where pending issues such as the proper choice of materials to prevent dielectric breakdown, the precise control of dopants inside semiconductors, the methodology of EUV lithography, the advanced metrologies to resolve finer spatial features, etc. remain the daunting technology challenges. On the other hand, current electronic devices only use the charge degree of freedom of electrons and proposals to tap into other degrees such as spin and/or orbital can be attractive because they offer additional dimensions to manipulate the digital information. But to realize these novel devices, one needs materials with two or more functionalities emerging from the interactions between multiple electronic degrees of freedom.

Materials that exhibit two or more ferroic orders, such as ferroelasticity, ferroelectricity, and ferromagnetism (or antiferromagnetism), are known as multiferroics. Although multiferroics can be attractive candidates for next generation electronic devices that will employ all electronic degrees of freedom, it is not easy to find them [1–5]. Taking the coexistence of ferroelectricity and ferromagnetism as an example, these two ferroic orders are quite different from the symmetry point of view: ferroelectricity is associated with broken inversion symmetry while ferromagnetism is associated with broken time-reversal symmetry. From the electronic point of view, partially filled *d* orbitals in transition metal elements are important for ferromagnetism, but ferroelectricity favors ions with empty *d* orbitals.

Recently, the so-called type-II multiferroic manganites $RMnO_3$ and RMn_2O_5 (*R*: rare earth elements) whose ferroelectricity is induced by complex magnetic orders have been demonstrated to exhibit strong

---

* Corresponding authors at: Advanced Light Source, Lawrence Berkeley National Laboratory, Berkeley, CA 94720, USA.
E-mail addresses: shih-wen.huang@maxiv.lu.se (S.-W. Huang), ychuang@lbl.gov (Y.-D. Chuang).

https://doi.org/10.1016/j.elspec.2020.147013
Received 25 June 2020; Received in revised form 27 October 2020; Accepted 28 October 2020
Available online 10 November 2020

magnetoelectric effect [6–14]. With respect to temperature, they often go through a series of magnetic transitions with distinct magnetic orders and electric properties, as illustrated in Fig. 1(a) for $DyMnO_3$. When subjected to magnetic field or electric field, their responses also vary significantly [15–18]. These multiferroic manganites offer us the opportunity to control one order through perturbations that influence the other electronic degree of freedom [1,19–23]. This aspect, in particular using electric field (charge degree of freedom) and magnetic field (spin degree of freedom) to control ferromagnetism and ferroelectricity, respectively, makes them extremely useful for electronic technologies because the flexibility in changing the charge and spin states of electrons provides other means to exchange and store digital information.

Several mechanisms, such as anti-symmetric inverse Dzyaloshinskii-Moriya (DM) interaction (spin current) [24–26], symmetric Heisenberg exchange interaction (exchange striction) [27–30], spin-dependent Mn-ligand *p-d* hybridization [31], and other degrees of freedom such as orbital and lattice [32–39], have been proposed to explain the ferroelectricity in these manganites [21,22]. Previously, we used resonant soft X-ray scattering (RSXS) spectroscopy to study the first harmonic *F*-type (0, τ, 0) diffraction peak produced by the sinusoidal antiferromagnetic spin order in multiferroic $DyMnO_3$ and $TbMnO_3$ to show that the aforementioned mechanisms can play different roles in the ferroelectric transitions. In particular, we pointed out that besides the structural based mechanisms, the electronic correlation is an important ingredient to understand the ferroelectricity in $DyMnO_3$ [40].

Here, we look at the second harmonic *C*-type (0, 1–2τ, 0) peak of $DyMnO_3$ measured at Mn L_2-edge. Compared with τ^{Mn} determined from first harmonic peak, τ^{Mn} from second harmonic peak tracks τ^{Dy} even more closely. Furthermore, the anomalous temperature dependence around the ferroelectric transition is also seen in the correlation length λ of second harmonic peak, corroborating with previous findings in first harmonic peak. By performing similar DFT calculations, we notice that the variant in magnetic ground states has weaker effect on the structure of $TbMnO_3$ compared to $DyMnO_3$. The calculations are consistent with the proposal that the proximity to E-type antiferromagnetism is an important factor in understanding the ferroelectricity in $DyMnO_3$ as well.

2. Results and discussions

Selected *q*-scans at O *K*- and Mn L_2-edges are shown in Fig. 1(b) and (c, d), respectively. Due to multiple absorption edges used in this study, we adopt the following convention to simplify the discussion: O, Mn, and Dy in the superscript of τ, *I*, and λ indicate the results from measurements at O *K*-, Mn L_2-, and Dy M_5-edges. 1 and 2 indicate the results for (0, τ, 0) (first harmonic) and (0, 1–2τ, 0) (second harmonic) diffraction peaks.

Below the Neel temperature T_N ~39 K, Mn spins form a collinear sinusoidal antiferromagnetic order along the crystalline $\widehat{b}$-axis. This magnetic order produces the first harmonic *F*-type (0, τ^{Mn}, 0) (Fig. 1(c), $h\nu$ = 645.4 eV) and second harmonic *C*-type (0, 1–2τ^{Mn}, 0) (Fig. 1(d), $h\nu$ = 645.8 eV) diffraction peaks that can be accessed using soft X-rays. The first harmonic directly comes from magnetic order from Mn sites while the second harmonic peak comes from the quadratic term in the magnetoelastic coupling between lattice and spin degrees of freedom, and are all influenced by Mn 3*d* orbitals. When the sample temperature

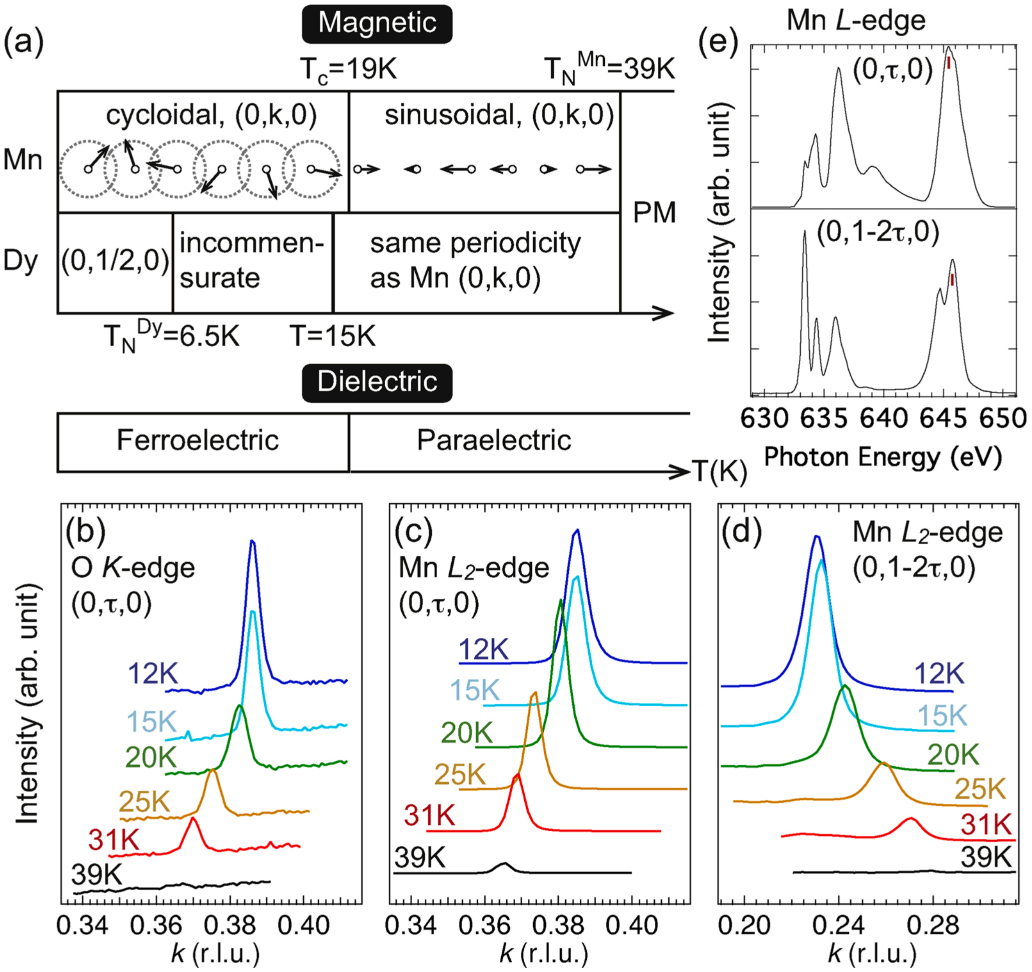

Fig. 1. (a) Schematic plot showing the characteristic temperatures for magnetic orders for Mn and Dy spins and the electric properties. (b–d) Normalized *q*-scans at selected temperatures for (b) *F*-type (0, τ^{O}, 0) at O *K*-edge (523.75 eV), (c) *F*-type (0, τ^{Mn}, 0) at Mn L_2-edge (645.4 eV) and (d) *C*-type (0, 1–2τ^{Mn}, 0) at Mn L_2-edge (645.8 eV). Spectra are shifted vertically for clarity. (e) $h\nu$-scans at (0, τ^{Mn}, 0) (top) and (0, 1–2τ^{Mn}, 0) (bottom) at 13 K, τ^{Mn} = 0.385. The red vertical ticks show the photon energies used in recording the *q*-scans in panels (c) and (d). (For interpretation of the references to color in this figure legend, the reader is referred to the web version of this article.)

is increased, like (0, $\tau^{\rm O}$, 0), both first and second harmonic peaks become weaker, consistent with the literatures [12,41–51]. However, close examination shows that they have different intensity and width behaviors: the (0, 1–2$\tau^{\rm Mn}$, 0) peak exhibits more drastic decrease in intensity above 20 K and has a broader width (or equivalently, shorter correlation length) throughout the temperature range. In Fig. 1(e), we show $h\nu$-scans at $(h,k,l) = (0, \tau^{\rm Mn}, 0)$ (top) and (0, 1–2$\tau^{\rm Mn}$, 0) (bottom) at $\tau^{\rm Mn} = 0.385$ and 13 K. From the distinct incident photon energy dependence (the resonance profile), it is clear that their contrasting behaviors are related to different electronic states involved in producing these diffraction peaks. To quantify the differences, the Lorentzian fitting was performed on q-scans and results are summarized in Fig. 2 (a)–(h).

We overlay $\tau^{\rm Mn}$s from (0, τ, 0) (blue open circles, $\tau^{\rm Mn,1}$) and (0, 1–2τ, 0) (green filled circles, $\tau^{\rm Mn,2}$) diffraction peaks with $\tau^{\rm Dy}$ from (0, τ, 0) peak (red filled diamonds) in Fig. 2(a) and (b), respectively. The difference $\Delta\tau = \tau^{\rm Dy}$-$\tau^{\rm Mn}$ is shown in the top panels. From the temperature dependence of $\Delta\tau$, one can see that $\tau^{\rm Mn,2}$ tracks $\tau^{\rm Dy}$ more closely than $\tau^{\rm Mn,1}$, with the magnitude of $\Delta\tau$ less than half of that of $\tau^{\rm Mn,1}$. The agreement can also be seen in the intensity and correlation length behaviors. The intensities $I^{\rm Mn,1}$ (Fig. 2(c)), $I^{\rm Mn,2}$ (Fig. 2(e)), and $I^{\rm Dy}$ (Fig. 2 (g)) all exhibit monotonic decrease with increasing sample temperature. A kink that marks the onset of linear temperature dependence at high temperature (the dashed color lines are guides for eyes) is observed in all curves around 20 ~25 K, just above the ferroelectric transition temperature $T_{\rm FE}$ = 19 K (the ferroelectric phase is shown as blue shaded region). However, the magnitude of this kink is much larger in $I^{\rm Mn,2}$ and $I^{\rm Dy}$. For $\lambda^{\rm Mn,1}$ (Fig. 2(d)), $\lambda^{\rm Mn,2}$ (Fig. 2(f)), and $\lambda^{\rm Dy}$ (Fig. 2(h)), they all show larger values above the ferroelectric transition, but the anomalous reduction seen in $\lambda^{\rm Dy}$ is also observed in $\lambda^{\rm Mn,2}$. Previously, we argued that this anomaly is not due to fitting artifacts and can be attributed to the symmetric exchange coupling $H_{\rm df} = g_{\mu_B}\Sigma_i \vec{s}_i \cdot \vec{H}_{\rm in}$ between Mn and Dy spins [40]. Observing similar behavior in $\lambda^{\rm Mn,2}$ that has comparable magnitude substantiates the authenticity of this anomaly. The similarity between the (0, 1–2τ, 0) peak measured at Mn L_2-edge and the (0, τ, 0) peak measured at Dy M_5-edge implies that the strong coupling between Mn and Dy spins involve Mn 3d orbitals as well.

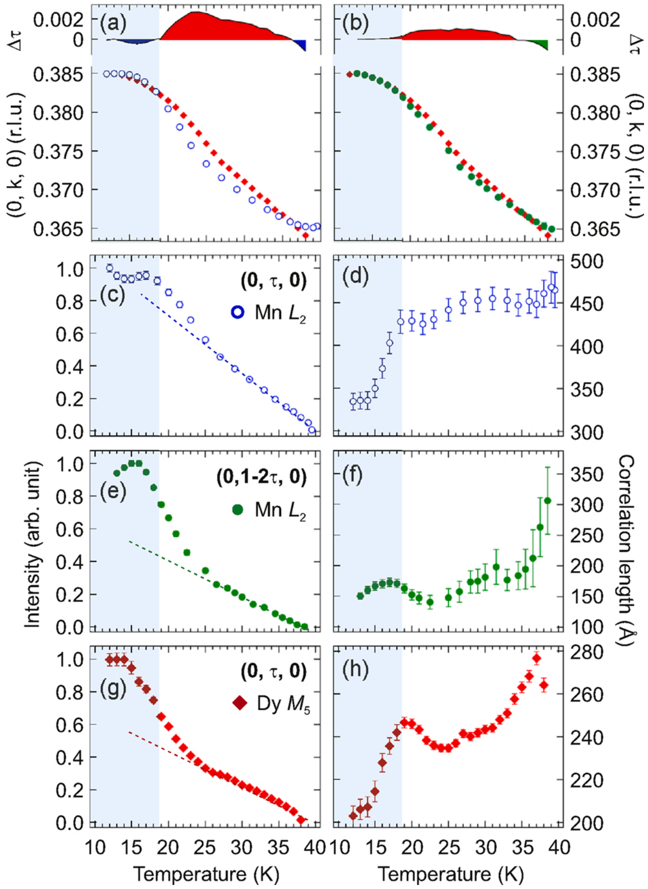

Fig. 2. Lorentzian fitting results of q-scans showing the temperature dependence of (a, b) ordering wave vectors τ, (c, e, g) peak intensities I, and (d, f, h) correlation lengths λ. (a) Comparison of $\tau^{\rm Dy}$ and $\tau^{\rm Mn,1}$. (b) Comparison of $\tau^{\rm Dy}$ and $\tau^{\rm Mn,2}$. Top panels in (a) and (b) show the difference $\Delta\tau = \tau^{\rm Dy}$-$\tau^{\rm Mn,1(2)}$. The $(\tau, I, \lambda)^{\rm Mn,1}$ (blue open circles), $(\tau, I, \lambda)^{\rm Mn,2}$ (green filled circles), and $(\tau, I, \lambda)^{\rm Dy}$ (red filled diamonds) are determined from F-type (0, τ, 0), C-type (0, 1–2τ, 0), and F-type (0, τ, 0) diffraction peaks measured at Mn L_2- (645.4 eV), Mn L_2- (645.8 eV), and Dy M_5-edges (1290 eV), respectively. The blue shaded area marks the ferroelectric phase. The dashed lines mark the linear temperature dependence at high temperature and are guides for eyes. (For interpretation of the references to color in this figure legend, the reader is referred to the web version of this article.)

Although DyMnO$_3$ and TbMnO$_3$ are the prototypical multiferroics that have been extensively studied over the past years, the former one has more than three times the electric polarization ($P_s \sim 0.2\,\mu$C/cm^2) than the latter one and is more attractive from the perspective of electronic technology applications. One plausible reason for the enhanced electric polarization is the coherence spin configuration of Mn and Dy below T_N. When going from La to Ho, the size of rare earth ion decreases; consequently, the lattice distortion is enhanced through tilting and deformation of MnO$_6$ octahedral. With enhanced lattice distortion, the strength of spin interactions are modified such that the magnetic ground state evolves from A-type (LaMnO$_3$) to collinear sinusoidal (Tb/DyMnO$_3$) to E-type antiferromagnetism (HoMnO$_3$) [7,9]. In addition, the tendency for orbital mixing and orbital ordering becomes stronger [52–54].

Previously, we carried out DFT calculations with A-type and E-type antiferromagnetism that do not naturally occur in DyMnO$_3$ and investigated the effect of magnetic ground states on Mn 3d orbitals. We showed that with E-type antiferromagnetism, the lattice structure is further distorted after relaxation with four inequivalent in-plane Mn-O bands, that leads to more delocalized O p orbitals. Based on that result, we argued that the proximity to E-type antiferromagnetism may enhance Mn and neighboring oxygen orbital hybridizations in DyMnO$_3$. Here, we perform similar DFT calculations on TbMnO$_3$ and compare results from DyMnO$_3$. The calculated spin polarized partial density of states (pDOS) of Mn in DyMnO$_3$ (left panels) and TbMnO$_3$ (right panels) are summarized in Fig. 3. In this figure, the A-type (top panels) and E-type (bottom panels) antiferromagnetism are employed with proper lattice relaxation to attain the ground states.

The DFT calculations reproduce the insulating ground states for both materials with similar Mn 3d pDOS (up and down arrows in the figure denote the majority and minority spins, respectively). Upon changing the magnetic ground state from A-type to E-type antiferromagnetism, the majority 3$d_{3x^2-r^2/3y^2-r^2}$ orbitals (blue) in valence band are pushed up in energy, resulting in more spectral weight near the top of valence band. In addition, the majority 3$d_{x^2-z^2/y^2-z^2}$ orbitals in conduction band become narrower. In fact, band-narrowing is a generic trend for Mn 3d orbitals with E-type antiferromagnetism for DyMnO$_3$ and TbMnO$_3$, and this effect pushes the rare earth d bands to even higher energy [data not shown in the figure].

Noticing that the band profiles can change significantly with respect to the magnetic ground states, we now look at their variants in the spatial distribution. The pDOS is integrated over [− 0.74 eV, 0 eV] energy window to produce the iso-charge surface, which are shown in Fig. 4. In this figure, we only show the results with relaxed E-type antiferromagnetism. The Mn-O bond lengths (Mn-O(1): out-of-plane bonds; Mn-O(2): in-plane bonds) for DyMnO$_3$ (DMO) and TbMnO$_3$ (TMO) using different magnetic ground states with and without lattice relaxation are summarized in Table 1. Like in previous study for

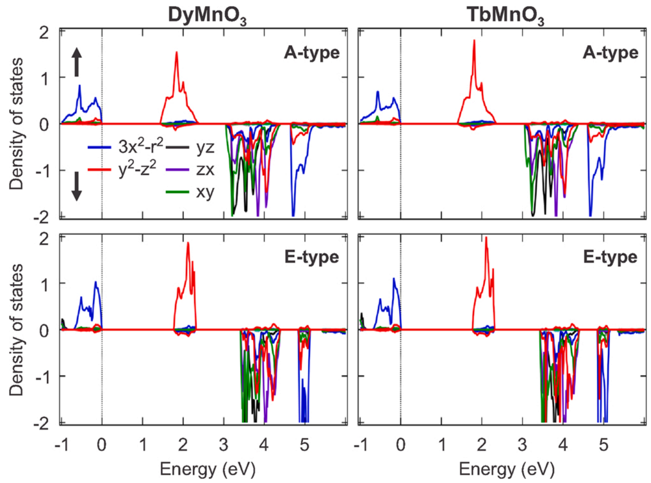

Fig. 3. Spin polarized partial density of states (pDOS) of Mn in DyMnO$_3$ (left) and TbMnO$_3$ (right) with A-type (top) and E-type (bottom) antiferromagnetism. The up and down arrows indicate the majority and minority spins, respectively. The Mn *s* and *p* orbitals are located at much higher energies outside the display window. (For interpretation of the references to color in this figure legend, the reader is referred to the web version of this article.)

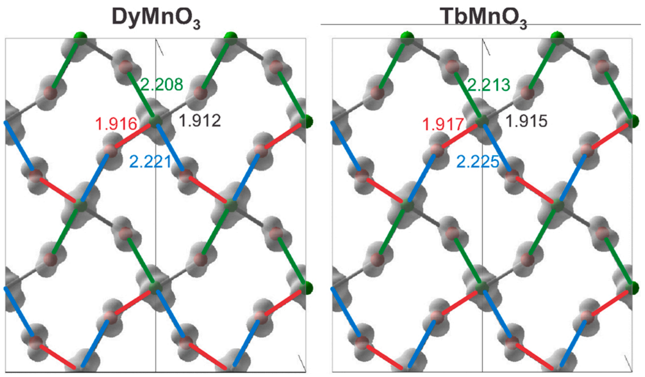

Fig. 4. The in-plane iso-charge surface of DyMnO$_3$ (left) and TbMnO$_3$ (right) with relaxed E-type antiferromagnetism. The iso-charge surface is produced by integrating the DFT density of states in [− 0.74 eV, 0 eV] energy window. (For interpretation of the references to color in this figure legend, the reader is referred to the web version of this article.)

DyMnO$_3$, [40] the lattice structure for TbMnO$_3$ also becomes more asymmetrically distorted in-plane when going from A-type to E-type antiferromagnetism, reflecting the loss of local mirror symmetry [the difference between two inequivalent Mn-O(2) bond pairs is increased from A-type to E-type antiferromagnetism]. In the meantime, the Mn 3*d* orbitals become more delocalized as expected. What is intriguing from DFT calculations is that for TbMnO$_3$, the effect of lattice relaxation with respect to different magnetic ground states is much smaller compared to DyMnO$_3$ (see boldface numbers in Table 1; numbers in () are the differences in the bond length without and with lattice relaxation). This implies that contrary to DyMnO$_3$, the exact choice of magnetic ground state (or proximity to A-type or E-type antiferromagnetism) plays a minor role in affecting the energetics of TbMnO$_3$. From previous study [40], we showed that the wave vector of F-type (0, τ, 0) diffraction peak for DyMnO$_3$ and TbMnO$_3$ displays contrasting temperature dependence where upon lowering the temperature, the former one increases continuously from 0.365 to 0.385 while the latter one reduces from 0.30 down to 0.285 at 17 K. Since DFT calculation shows that the choice of exact magnetic ground state has a weaker effect on the structure of TbMnO$_3$ relative to DyMnO$_3$, it is reasonable to expect that the wave vector of TbMnO$_3$ magnetic order can deviate from the E-type antiferromagnetism (wave vector around 0.354) without the significant energetic penalty from the spin-lattice interaction. On the other hand, the tracking of the wave vector of C-type (0, 1–2τ, 0) (from magnetoelastic coupling) of Mn spin and F-type (0, τ, 0) of Dy spin (Fig. 2(b)) reflects the important role of structural influence that keeps these wave vectors around that of the E-type antiferromagnetism.

3. Summary

We have used RSXS spectroscopy to study the second harmonic *C*-type (0, 1–2τ, 0) diffraction peak in multiferroic DyMnO$_3$. We show that the wave vector of sinusoidal antiferromagnetic spin order determined from this second harmonic peak at Mn L_2-edge ($\tau^{\mathrm{Mn},2}$) tracks that of the first harmonic peak at Dy M_5-edge (τ^{Dy}) much more closely. Furthermore, the anomalous reduction in the correlation length just above the ferroelectric transition seen previously in λ^{Dy} is also observed in $\lambda^{\mathrm{Mn},2}$. The similarity between these two diffraction peaks implies that the strong coupling between Mn and Dy spins has noticeable Mn 3*d* orbital involvement. We also carry out DFT calculations to look at the effect of different magnetic ground states on Mn 3*d* orbitals. Contrary to DyMnO$_3$, we notice that the lattice response to different antiferromagnetic ground states with and without lattice relaxation is much smaller in TbMnO$_3$. The weak response is in agreement with the notion that the proximity to E-type antiferromagnetism plays a more important role in DyMnO$_3$ than TbMnO$_3$.

4. Materials and methods

Single crystal DyMnO$_3$ was grown by flux method and the details of crystal growth can be found elsewhere [55,56]. The crystal was checked by conventional four-circle diffractometry to confirm the orthorhombically distorted perovskite structure with *Pbnm* space group (a = 5.28 Å, b = 5.85 Å, c = 7.38 Å). Since the natural growth produces the [1, 1, 0] surface, the [0, 1, 0] and [0, 0, 1] surfaces were aligned in the horizontal scattering plane by mounting the sample on a 45° wedge. RSXS measurements were carried out at Beamline 8.0.1 at the Advanced Light Source (ALS), Lawrence Berkeley National Laboratory (LBNL), using the RSXS endstation [57]. During measurements, the incident photon polarization was kept in the horizontal scattering plane (π-scattering geometry). The beamline energy resolution was better than 0.3 eV, 0.25 eV, and 0.2 eV at O *K*- (523.75 eV), Mn L_2-

Table 1
Mn-O bond length from first principles calculations; () is the difference between relaxed and unrelaxed bond length; TMO and DMO stand for TbMnO$_3$ and DyMnO$_3$, respectively.

	Mn-O(1) (Å)	Mn-O(1) (Å)	Mn-O(2) (Å)	Mn-O(2) (Å)	Mn-O(2) (Å)	Mn-O(2) (Å)
A-/E-AF, unrelaxed DMO	1.938	1.938	1.883	1.883	2.24	2.24
A-AF relaxed DMO	1.957 (0.019)	1.957 (0.019)	1.92 (0.037)	1.92 (0.037)	2.207 (− 0.033)	2.207 (− 0.033)
E-AF relaxed DMO	1.953 (0.015)	1.954 (0.016)	1.912 (**0.029**)	1.916 (**0.033**)	2.208(− **0.032**)	2.221(− **0.019**)
A-/E-AF, unrelaxed TMO	1.939	1.939	1.908	1.908	2.214	2.214
A-AF relaxed TMO	1.956 (0.017)	1.956 (0.017)	1.923(0.015)	1.923(0.015)	2.209 (− 0.005)	2.209 (− 0.005)
E-AF relaxed TMO	1.955 (0.016)	1.956 (0.017)	1.915(**0.007**)	1.917(**0.009**)	2.213 (− **0.001**)	2.225 (**0.011**)

(645.4 eV/645.8 eV), and Dy M_5-edges (1290 eV), respectively. The beam spot on the sample was around 40 μm (v) by 500 μm (h). All temperature dependence spectra were recorded in the warming process.

A photodiode with front Al window to block out ambient light and photoelectrons was used to record the scattered X-rays from sample. The angular resolution of this photodiode was ∼0.5°, better than the half-width half-maximum (HWHM) of diffraction peaks. Two types of spectra were recorded and presented in this paper: $h\nu$- and q-scans. For q-scans, the incident photon energy was fixed while sample (θ) and detector angles were varied so that photon momentum transfer was projected along the crystalline $\widehat{b}$-axis. In the current study, the sample and detector angles followed θ-2θ relationship. For $h\nu$-scans, the incident photon energy, sample, and detector angles were changed simultaneously to keep the photon momentum transfer at a specific $\overrightarrow{q}$-value. The q-scans were first normalized by incident photon flux determined from the photocurrent of an upstream Au mesh. The normalized spectra were then fitted with a Lorentzian function on top of a linear background to remove the contributions from fluorescence and specular reflection [these two contributions have monotonic $\overrightarrow{q}$ dependence]. The ordering wave vector τ was determined from the peak position. The intensity I shown in this paper is the peak area. The correlation length λ was calculated using the inverse of half-width half-maximum (HWHM) of Lorentzian peak.

The first principles calculations were carried using the accurate full-potential augmented-wave method [58,59], as embodied in the Vienna *ab initial* simulation package (VASP). The exchange-correlation initiation was treated within the generalized gradient approximation (GGA+U). The calculations were performed over $7 \times 7 \times 5$ ($a \times b \times c$ unit cell) and $7 \times 3 \times 5$ ($a \times 2b \times c$ unit cell) Monkhorst-Pack k-point meshes in the irreducible Brillouin zone for A- and E-type antiferromagnetism, respectively. Lattice relaxation, which gives lower energy, was also included in the calculations. The on-site Coulomb energy U = 5.0 eV and exchange energy J = 0.87 eV were used for Mn 3d electrons [56].

Declaration of Competing Interest

The authors report no declarations of interest.

Acknowledgement

The Advanced Light Source is supported by the Director, Office of Science, Office of Basic Energy Sciences, of the U.S. Department of Energy under Contract No. DE-AC02-05CH11231. Work by J. Y. L. was financially supported by the MOST of Taiwan, under the Grant 103-2112-M-009-007-MY3 and the Center for Emergent Functional Matter Science of National Chiao Tung University from The Featured Areas Research Center Program within the framework of the Higher Education Sprout Project by the Ministry of Education (MOE) in Taiwan.

References

[1] N.A. Spaldin, M. Fiebig, The renaissance of magnetoelectric multiferroics, Science 309 (5733) (2005) 391–392, https://doi.org/10.1126/science.1113357.
[2] C. RayanáSerrao, et al., New routes to multiferroics, J. Mater. Chem. 17 (47) (2007) 4931–4938, https://doi.org/10.1039/B709126E.
[3] W. Eerenstein, N. Mathur, J.F. Scott, Multiferroic and magnetoelectric materials, Nature 442 (7104) (2006) 759–765, https://doi.org/10.1038/nature05023.
[4] J. Scott, Applications of modern ferroelectrics, Science 315 (5814) (2007) 954–959, https://doi.org/10.1126/science.1129564.
[5] R. Ramesh, Emerging routes to multiferroics, Nature 461 (7268) (2009) 1218–1219, https://doi.org/10.1038/4611218a.
[6] T. Kimura, T. Goto, H. Shintani, K. Ishizaka, T. Arima, Y. Tokura, Magnetic control of ferroelectric polarization, Nature 426 (6962) (2003) 55–58, https://doi.org/10.1038/nature02018.
[7] T. Kimura, S. Ishihara, H. Shintani, T. Arima, K.T. Takahashi, K. Ishizaka, Y. Tokura, Distorted perovskite with e_g^1 configuration as a frustrated spin system, Phys. Rev. B 68 (2003) 060403, https://doi.org/10.1103/PhysRevB.68.060403.
[8] N. Hur, S. Park, P. Sharma, J. Ahn, S. Guha, S.-W. Cheong, Electric polarization reversal and memory in a multiferroic material induced by magnetic fields, Nature 429 (6990) (2004) 392–395, https://doi.org/10.1038/nature02572.
[9] T. Goto, T. Kimura, G. Lawes, A.P. Ramirez, Y. Tokura, Ferroelectricity and giant magnetocapacitance in perovskite rare-earth manganites, Phys. Rev. Lett. 92 (2004) 257201, https://doi.org/10.1103/PhysRevLett.92.257201.
[10] T. Kimura, G. Lawes, T. Goto, Y. Tokura, A.P. Ramirez, Magnetoelectric phase diagrams of orthorhombic $RMnO_3$ (r = Gd, Tb, and Dy), Phys. Rev. B 71 (2005) 224425, https://doi.org/10.1103/PhysRevB.71.224425.
[11] M. Kenzelmann, A.B. Harris, S. Jonas, C. Broholm, J. Schefer, S.B. Kim, C.L. Zhang, S.-W. Cheong, O.P. Vajk, J.W. Lynn, Magnetic inversion symmetry breaking and ferroelectricity in $TbMnO_3$, Phys. Rev. Lett. 95 (2005) 087206, https://doi.org/10.1103/PhysRevLett.95.087206.
[12] R. Feyerherm, E. Dudzik, N. Aliouane, D.N. Argyriou, Commensurate Dy magnetic ordering associated with incommensurate lattice distortion in multiferroic $DyMnO_3$, Phys. Rev. B 73 (2006) 180401, https://doi.org/10.1103/PhysRevB.73.180401.
[13] T. Arima, T. Goto, Y. Yamasaki, S. Miyasaka, K. Ishii, M. Tsubota, T. Inami, Y. Murakami, Y. Tokura, Magnetic-field-induced transition in the lattice modulation of colossal magnetoelectric $GdMnO_3$ and $TbMnO_3$ compounds, Phys. Rev. B 72 (2005) 100102, https://doi.org/10.1103/PhysRevB.72.100102.
[14] T. Arima, A. Tokunaga, T. Goto, H. Kimura, Y. Noda, Y. Tokura, Collinear to spiral spin transformation without changing the modulation wavelength upon ferroelectric transition in $Tb_{1-x}Dy_xMnO_3$, Phys. Rev. Lett. 96 (2006) 097202, https://doi.org/10.1103/PhysRevLett.96.097202.
[15] N. Aliouane, D.N. Argyriou, J. Strempfer, I. Zegkinoglou, S. Landsgesell, M. V. Zimmermann, Field-induced linear magnetoelastic coupling in multiferroic $TbMnO_3$, Phys. Rev. B 73 (2006) 020102, https://doi.org/10.1103/PhysRevB.73.020102.
[16] D.N. Argyriou, N. Aliouane, J. Strempfer, I. Zegkinoglou, B. Bohnenbuck, K. Habicht, M.V. Zimmermann, Melting of incommensurate-ferroelectric phase with magnetic field in multiferroic $TbMnO_3$, Phys. Rev. B 75 (2007) 020101, https://doi.org/10.1103/PhysRevB.75.020101.
[17] J. Strempfer, B. Bohnenbuck, M. Mostovoy, N. Aliouane, D.N. Argyriou, F. Schrettle, J. Hemberger, A. Krimmel, M.V. Zimmermann, Absence of commensurate ordering at the polarization flop transition in multiferroic $DyMnO_3$, Phys. Rev. B 75 (2007) 212402, https://doi.org/10.1103/PhysRevB.75.212402.
[18] R. Feyerherm, E. Dudzik, A.U.B. Wolter, S. Valencia, O. Prokhnenko, A. Maljuk, S. Landsgesell, N. Aliouane, L. Bouchenoire, S. Brown, D.N. Argyriou, Magnetic-field induced effects on the electric polarization in $RMnO_3$ (R = Dy, Gd), Phys. Rev. B 79 (2009) 134426, https://doi.org/10.1103/PhysRevB.79.134426.
[19] S.-W. Cheong, M. Mostovoy, Multiferroics: a magnetic twist for ferroelectricity, Nat. Mater. 6 (1) (2007) 13–20, https://doi.org/10.1038/nmat1804.
[20] T. Kimura, Spiral magnets as magnetoelectrics, Annu. Rev. Mater. Res. 37 (2007) 387–413.
[21] Y. Tokura, S. Seki, Multiferroics with spiral spin orders, Adv. Mater. 22 (14) (2010) 1554–1565, https://doi.org/10.1002/adma.200901961.
[22] Y. Tokura, S. Seki, N. Nagaosa, Multiferroics of spin origin, Rep. Prog. Phys. 77 (7) (2014) 076501, https://doi.org/10.1088/0034-4885/77/7/076501.
[23] Y. Yamasaki, H. Sagayama, T. Goto, M. Matsuura, K. Hirota, T. Arima, Y. Tokura, Electric control of spin helicity in a magnetic ferroelectric, Phys. Rev. Lett. 98 (2007) 147204, https://doi.org/10.1103/PhysRevLett.98.147204.
[24] H. Katsura, N. Nagaosa, A.V. Balatsky, Spin current and magnetoelectric effect in noncollinear magnets, Phys. Rev. Lett. 95 (2005) 057205, https://doi.org/10.1103/PhysRevLett.95.057205.
[25] M. Mostovoy, Ferroelectricity in spiral magnets, Phys. Rev. Lett. 96 (2006) 067601, https://doi.org/10.1103/PhysRevLett.96.067601.
[26] I.A. Sergienko, E. Dagotto, Role of the Dzyaloshinskii-Moriya interaction in multiferroic perovskites, Phys. Rev. B 73 (2006) 094434, https://doi.org/10.1103/PhysRevB.73.094434.
[27] M. Mochizuki, N. Furukawa, Microscopic model and phase diagrams of the multiferroic perovskite manganites, Phys. Rev. B 80 (2009) 134416, https://doi.org/10.1103/PhysRevB.80.134416.
[28] M. Mochizuki, N. Furukawa, N. Nagaosa, Spin model of magnetostrictions in multiferroic Mn perovskites, Phys. Rev. Lett. 105 (2010) 037205, https://doi.org/10.1103/PhysRevLett.105.037205.
[29] M. Mochizuki, N. Furukawa, Theory of magnetic switching of ferroelectricity in spiral magnets, Phys. Rev. Lett. 105 (2010) 187601, https://doi.org/10.1103/PhysRevLett.105.187601.
[30] S. Ishiwata, Y. Kaneko, Y. Tokunaga, Y. Taguchi, T.-H. Arima, Y. Tokura, Perovskite manganites hosting versatile multiferroic phases with symmetric and antisymmetric exchange strictions, Phys. Rev. B 81 (2010) 100411, https://doi.org/10.1103/PhysRevB.81.100411.
[31] C. Jia, S. Onoda, N. Nagaosa, J.H. Han, Microscopic theory of spin-polarization coupling in multiferroic transition metal oxides, Phys. Rev. B 76 (2007) 144424, https://doi.org/10.1103/PhysRevB.76.144424.
[32] D.V. Efremov, J. Van Den Brink, D.I. Khomskii, Bond-versus site-centred ordering and possible ferroelectricity in manganites, Nat. Mater. 3 (12) (2004) 853–856, https://doi.org/10.1038/nmat1236.
[33] S. Picozzi, K. Yamauchi, B. Sanyal, I.A. Sergienko, E. Dagotto, Dual nature of improper ferroelectricity in a magnetoelectric multiferroic, Phys. Rev. Lett. 99 (2007) 227201, https://doi.org/10.1103/PhysRevLett.99.227201.
[34] J.J. Betouras, G. Giovannetti, J. van den Brink, Multiferroicity induced by dislocated spin-density waves, Phys. Rev. Lett. 98 (2007) 257602, https://doi.org/10.1103/PhysRevLett.98.257602.

[35] S. Dong, R. Yu, S. Yunoki, J.-M. Liu, E. Dagotto, Origin of multiferroic spiral spin order in the $RMnO_3$ perovskites, Phys. Rev. B 78 (2008) 155121, https://doi.org/10.1103/PhysRevB.78.155121.

[36] S. Dong, R. Yu, J.-M. Liu, E. Dagotto, Striped multiferroic phase in double-exchange model for quarter-doped manganites, Phys. Rev. Lett. 103 (2009) 107204, https://doi.org/10.1103/PhysRevLett.103.107204.

[37] B.H. Kim, B.I. Min, Nearest and next-nearest superexchange interactions in orthorhombic perovskite manganites $RMnO_3$ ($r =$ rare earth), Phys. Rev. B 80 (2009) 064416, https://doi.org/10.1103/PhysRevB.80.064416.

[38] J.L. Ribeiro, L.G. Vieira, Landau model for the phase diagrams of the orthorhombic rare-earth manganites $RMnO_3$ ($r =$ Eu, Gd, Tb, Dy, Ho), Phys. Rev. B 82 (2010) 064410, https://doi.org/10.1103/PhysRevB.82.064410.

[39] M. Mochizuki, N. Furukawa, N. Nagaosa, Theory of spin-phonon coupling in multiferroic manganese perovskites $RMnO_3$, Phys. Rev. B 84 (2011) 144409, https://doi.org/10.1103/PhysRevB.84.144409.

[40] S.W. Huang, J.M. Lee, H.-T. Jeng, Y. Shao, L.A. Wray, J.M. Chen, R. Qiao, W. L. Yang, Y. Cao, J.-Y. Lin, R.W. Schoenlein, Y.-D. Chuang, Prominent role of oxygen in the multiferroicity of $DyMnO_3$ and $TbMnO_3$: a resonant soft X-ray scattering spectroscopy study, Phys. Rev. B 94 (2016) 035145, https://doi.org/10.1103/PhysRevB.94.035145.

[41] O. Prokhnenko, R. Feyerherm, E. Dudzik, S. Landsgesell, N. Aliouane, L.C. Chapon, D.N. Argyriou, Enhanced ferroelectric polarization by induced dy spin order in multiferroic $DyMnO_3$, Phys. Rev. Lett. 98 (2007) 057206, https://doi.org/10.1103/PhysRevLett.98.057206.

[42] O. Prokhnenko, R. Feyerherm, M. Mostovoy, N. Aliouane, E. Dudzik, A.U. B. Wolter, A. Maljuk, D.N. Argyriou, Coupling of frustrated ising spins to the magnetic cycloid in multiferroic $TbMnO_3$, Phys. Rev. Lett. 99 (2007) 177206, https://doi.org/10.1103/PhysRevLett.99.177206.

[43] J. Strempfer, B. Bohnenbuck, I. Zegkinoglou, N. Aliouane, S. Landsgesell, M. V. Zimmermann, D.N. Argyriou, Magnetic-field-induced transitions in multiferroic $TbMnO_3$ probed by resonant and nonresonant X-ray diffraction, Phys. Rev. B 78 (2008) 024429, https://doi.org/10.1103/PhysRevB.78.024429.

[44] J. Voigt, J. Persson, J.W. Kim, G. Bihlmayer, T. Brückel, Strong coupling between the spin polarization of Mn and Tb in multiferroic $TbMnO_3$ determined by X-ray resonance exchange scattering, Phys. Rev. B 76 (2007) 104431, https://doi.org/10.1103/PhysRevB.76.104431.

[45] N. Aliouane, O. Prokhnenko, R. Feyerherm, M. Mostovoy, J. Strempfer, K. Habicht, K.C. Rule, E. Dudzik, A.U.B. Wolter, A. Maljuk, D.N. Argyriou, Magnetic order and ferroelectricity in $RMnO_3$ multiferroic manganites: coupling between R- and Mn-spins, J. Phys.: Condens. Matter 20 (43) (2008) 434215, https://doi.org/10.1088/0953-8984/20/43/434215.

[46] R.A. Ewings, A.T. Boothroyd, D.F. McMorrow, D. Mannix, H.C. Walker, B.M. R. Wanklyn, X-ray resonant diffraction study of multiferroic DyM_n2O_5, Phys. Rev. B 77 (2008) 104415, https://doi.org/10.1103/PhysRevB.77.104415.

[47] T. Forrest, S. Bland, S. Wilkins, H. Walker, T. Beale, P. Hatton, D. Prabhakaran, A. Boothroyd, D. Mannix, F. Yakhou, et al., Ordering of localized electronic states in multiferroic $TbMnO_3$: a soft X-ray resonant scattering study, J. Phys.: Condens. Matter 20 (42) (2008) 422205.

[48] S.B. Wilkins, T.R. Forrest, T.A.W. Beale, S.R. Bland, H.C. Walker, D. Mannix, F. Yakhou, D. Prabhakaran, A.T. Boothroyd, J.P. Hill, P.D. Hatton, D.F. McMorrow, Nature of the magnetic order and origin of induced ferroelectricity in $TbMnO_3$, Phys. Rev. Lett. 103 (2009) 207602, https://doi.org/10.1103/PhysRevLett.103.207602.

[49] T.A.W. Beale, S.B. Wilkins, R.D. Johnson, S.R. Bland, Y. Joly, T.R. Forrest, D. F. McMorrow, F. Yakhou, D. Prabhakaran, A.T. Boothroyd, P.D. Hatton, Antiferromagnetically spin polarized oxygen observed in magnetoelectric $TbMn_2O_5$, Phys. Rev. Lett. 105 (2010) 087203, https://doi.org/10.1103/PhysRevLett.105.087203.

[50] E. Schierle, V. Soltwisch, D. Schmitz, R. Feyerherm, A. Maljuk, F. Yokaichiya, D. N. Argyriou, E. Weschke, Cycloidal order of $4f$ moments as a probe of chiral domains in $ErMn_2O_5$, Phys. Rev. Lett. 105 (2010) 167207, https://doi.org/10.1103/PhysRevLett.105.167207.

[51] U. Staub, Y. Bodenthin, M. García-Fernández, R.A. de Souza, M. Garganourakis, E. I. Golovenchits, V.A. Sanina, S.G. Lushnikov, Magnetic order of multiferroic $ErMn_2O_5$ studied by resonant soft X-ray bragg diffraction, Phys. Rev. B 81 (2010) 144401, https://doi.org/10.1103/PhysRevB.81.144401.

[52] G. Maris, V. Volotchaev, T. Palstra, Effect of ionic size on the orbital ordering transition in $RMnO_{3+\delta}$, New J. Phys. 6 (1) (2004) 153, https://doi.org/10.1088/1367-2630/6/1/153.

[53] M.W. Kim, S.J. Moon, J.H. Jung, J. Yu, S. Parashar, P. Murugavel, J.H. Lee, T. W. Noh, Effect of orbital rotation and mixing on the optical properties of orthorhombic $RMnO_3$ ($r =$ La, Pr, Nd, Gd, and Tb), Phys. Rev. Lett. 96 (2006) 247205, https://doi.org/10.1103/PhysRevLett.96.247205.

[54] F.-K. Chiang, M.-W. Chu, F.C. Chou, H.T. Jeng, H.S. Sheu, F.R. Chen, C.H. Chen, Effect of Jahn-Teller distortion on magnetic ordering in $Dy(Fe,Mn)O_3$ perovskites, Phys. Rev. B 83 (2011) 245105, https://doi.org/10.1103/PhysRevB.83.245105.

[55] J. Chen, C. Chen, T. Chou, I. Jarrige, H. Ishii, K. Lu, Y. Cai, K. Liang, J. Lee, S. Huang, et al., Resonant X-ray emission spectroscopy of multiferroic $TbMnO_3$, Appl. Phys. Lett. 91 (5) (2007) 054108, https://doi.org/10.1063/1.2762288.

[56] J.M. Chen, Z. Hu, H.T. Jeng, Y.Y. Chin, J.M. Lee, S.W. Huang, K.T. Lu, C.K. Chen, S. C. Haw, T.L. Chou, H.-J. Lin, C.C. Shen, R.S. Liu, A. Tanaka, L.H. Tjeng, C.T. Chen, Strong orbital polarization in orthorhombic $DyMnO_3$: a combined X-ray linear dichroism and ab initio electronic structure study, Phys. Rev. B 81 (2010) 201102, https://doi.org/10.1103/PhysRevB.81.201102.

[57] D. Doering, Y.-D. Chuang, N. Andresen, K. Chow, D. Contarato, C. Cummings, E. Domning, J. Joseph, J. Pepper, B. Smith, et al., Development of a compact fast ccd camera and resonant soft X-ray scattering endstation for time-resolved pump-probe experiments, Rev. Sci. Instrum. 82 (7) (2011) 073303, https://doi.org/10.1063/1.3609862.

[58] P.E. Blöchl, Projector augmented-wave method, Phys. Rev. B 50 (1994) 17953–17979, https://doi.org/10.1103/PhysRevB.50.17953.

[59] G. Kresse, D. Joubert, From ultrasoft pseudopotentials to the projector augmented-wave method, Phys. Rev. B 59 (1999) 1758–1775, https://doi.org/10.1103/PhysRevB.59.1758.